Journal of Solid State Chemistry **148,** 468–478 (1999)
Article ID jssc.1999.8482, available online at http://www.idealibrary.com on IDEAL®

Spectroscopic Properties and Magnetic Phase Transitions in Scheelite $M^{I}Cr(MoO_4)_2$ and Wolframite $M^{I}Cr(WO_4)_2$ Crystals, where M^{I} = Li, Na, K, and Cs

J. Hanuza,[1] M. Mączka, K. Hermanowicz, P. J. Dereń, W. Stręk, L. Folcik, and H. Drulis

Institute for Low Temperature and Structure Research, Polish Academy of Sciences, Wrocław, Poland

Received February 8, 1999; in revised form July 16, 1999; accepted August 11, 1999

We present a spectroscopic overview of Cr^{3+} ions in $M^{I}Cr(MO_4)_2$ scheelites, a prospective crystals lasing in the infrared region, and new magnetic materials exhibiting antiferromagnetic ordering (M^{I} = Li, Na, K, Cs and M = Mo and W). The infrared, Raman, electronic absorption, and fluorescence measurements were conducted at temperatures ranging from 77 to 300 K. The ESR, magnetic susceptibility, and magnetic field dependence were studied in the 4–300 K range and discussed in terms of Cr^{3+} ion properties in these compounds. The magnetic transitions are reported for all compounds studied. © 1999 Academic Press

INTRODUCTION

Recent research in tunable solid state lasers has discovered a new class of materials that shows laser action in the NIR region. The successful demonstration of the emission from chromium (IV) ion in forsterite Mg_2SiO_4 and YAG (1–5) has created interest in other materials that might show similar behavior and can be used to penetrate other wavelength regions. Molybdates and tungstates with scheelite structure are important host crystals for a variety of inorganic phosphors and therefore are of interest as laser materials (6, 7). The tetragonal crystals of the formula $M^{II}XO_4$ (X = Mo, W and M^{II} = Ca, Pb, Mg) have interesting structural and physicochemical properties. With decreasing temperature some of them undergo a phase transition to monoclinic pseudoscheelite structure (8–10). They may have domain structure in the ferroelastic phase. In several scheelite crystals the phase transition may be induced by pressure (11, 12). The compounds of $M^{I}M^{III}(XO_4)_2$ stoichiometry are particularly promising as laser media because the M^{III} ions (Sc, In, Al, La, Y) can be easily replaced by active dopants (1).

[1]To whom correspondence should be addressed. Fax: (48-71) 441 029. E-mail: hanuza@int.pan.wroc.pl.

The present paper deals with scheelite-type double molybdates and wolframite-type tungstates of the formula $M^{I}Cr(XO_4)_2$. Their structure is derived by substituting M^{II} sites of $M^{II}XO_4$ scheelites by M^{I} alkaline earth and Cr^{3+} ions. These ions can statistically occupy two positions of the unit cell with different occupancy factors (13). In this structure the appearance of local deviations from statistical ordering of the cationic layers has very important consequences. This domain structure of the scheelite-like crystals seems to be their characteristic feature.

In the present paper we have examined the optical spectra of fully concentrated $M^{I}Cr(XO_4)_2$ in the FIR, IR, MIR, and visible regions by means of absorption and emission measurements. The ESR and magnetic susceptibility are also studied and discussed. The nature of the magnetic transitions is analyzed. An overview of the basic spectroscopic and magnetic features is given together with the physical model that can explain our data.

EXPERIMENTAL

A. Preparation of the Single Crystals

The alkali metal–chromium double molybdates and tungstates were prepared by the flux method. Starting materials were $M^{I}_2CO_3$, Cr_2O_3, and MoO_3 (WO_3), where M^{I} = Li, Na, K, Cs. Mixtures of the appropriate contents, placed in platinum crucibles, were heated in a furnace up to 800°C for the double molybdates and 1000°C for the tungstates. The reaction mixtures were kept at these temperatures for 20 h, cooled at 2°C per hour to 500°C, and then cooled at 5°C/h to room-temperature. The synthesized crystals were washed up from the solvent ($M^{I}_2Mo_2O_7$ or $M^{I}_2W_2O_7$) with boiling water. The $NaCr(MoO_4)_2$ and $KCr(MoO_4)_2$ crystals are dark green and the other remaining crystals are dark violet. The stoichiometry of the crystal studied was confirmed by means of chemical analysis.

0022-4596/99 $30.00
Copyright © 1999 by Academic Press
All rights of reproduction in any form reserved.

B. Experimental Details

IR spectra in the range 50–4000 cm^{-1} were recorded in nujol and KBr suspensions with Bruker IFS 88 and Perkin–Elmer 200 FT-IR spectrometers. The resolution was 1 cm^{-1} in the IR range and 2 cm^{-1} in the far-infrared one.

Raman spectra were measured in 90° scattering geometry. The excitation source was the 488 nm line of an Ar^+ ion laser with an output power of 150 mW. The monochromator was a double grating model DFS-24 ($f = 0.8$ m) with a photon counting detection system–cooled GaAs Burle (USA) photomultiplier. The resolution was 2 cm^{-1}.

Electronic diffuse reflectance (DR) spectra in the UV-visible region (200–850 nm) were collected with a Specord 500 Carll Zeiss spectrophotometer equipped with a reflectance attachment. The resolution was 1 nm. The samples were pressed into disks and $BaSO_4$ was used as reference material. The absorption spectra were measured in a Cary 5E spectrophotometer.

The emission spectra were recorded on a THR 1000 Jobin Yvon monochromator. A highly sensitive photomultiplier (R928—Hamamatsu) was used for detecting the spin forbidden transition as well as the decay profiles. A PbS detector cooled with dry ice was used to detect the emission spectra in the near IR region. A SR400 from Stanford—photon counting system—served for measurements of the decay profiles. A close cycled helium cryostat was used to cool down the samples (to 15 K). An excimer laser (from Lambda Physik) and a krypton laser (from Carl Zeiss Jena) were used as the excitation sources.

Magnetization and dc magnetic susceptibility measurements were performed on polycrystalline samples in the temperature interval 1.7–300 K and in applied magnetic fields up to 55000 G using a Quantum Design MPMS-5 SQUID magnetometer.

ESR spectra in the polycrystalline state were measured in the 4.3–300 K temperature range with an X-band Radiopan Spectrometer. The magnetic field was calibrated with a nuclear MJ110R magnetometer.

RESULTS AND DISCUSSION

A. Crystal Structure

$LiCr(MoO_4)_2$ crystallizes in the triclinic space group $P\bar{1}$ (C_i^1) with $Z = 2$ (14) and is isostructural with $LiAl(MoO_4)_2$ phase for which $a = 7.10$ Å, $b = 7.25$ Å, $c = 6.67$ Å, $\alpha = 111°$, $\beta = 105°$, $\gamma = 90°$ (15). The structure of this compound consists of both isolated MoO_4 tetrahedra and Mo_2O_8 dimers. For some Mo atoms the coordination number (CN) is four, and for others it is five. The Li^+, Cr^{3+}, and Mo^{6+} ions occupy sites of C_1 symmetry.

$NaCr(MoO_4)_2$ is isostructural to $NaFe(MoO_4)_2$ (16) and crystallizes in the monoclinic space group $C2/c$ (C_{2h}^6); $a = 9.80$ Å, $b = 5.26$ Å, $c = 13.55$ Å, $\beta = 90.4°$, and $Z = 4$ (14). The crystal structure of potassium–chromium double molybdate is not given in the literature. However, because the phonon spectra of $NaCr(MoO_4)_2$ and $KCr(MoO_4)_2$, are nearby the same, it should be assumed that these compounds are isostructural. As in the case of $LiCr(MoO_4)_2$, the MoO_4 and Mo_2O_8 units exist in the unit cell. The coordination number of the chromium atoms is 6. The Na, Cr, and Mo atoms occupy sites of C_2, C_i, and C_1 symmetry, respectively.

According to studies by Trunov and Efremov (17), $CsCr(MoO_4)_2$ crystallizes in the trigonal structure with $a = 5.577$ Å, $c = 8.056$ Å. Lattice parameters are given in works by Kelvtsov and Klevtsova (18), where the structure is described as hexagonal $P\bar{3}ml$ (D_{3d}^3), being isostructural with $KAl(MoO_4)_2$. From the spectroscopic point of view this structure is the most probable. The basic units of this structure are isolated molybdate tetrahedra. The Cs^+, Cr^{3+} ions occupy sites of D_{3d} symmetry and those of Mo^{6+} sites of C_{3v} symmetry.

$NaCr(WO_4)_2$ tungstate crystallizes in wolframite-type structure $P2/c$ (C_{2h}^4) with two formula per unit cell, being isostructural with $NaIn(WO_4)_2$ for which $a = 10.08$ Å, $b = 5.81$ Å, $c = 5.03$ Å, and $\beta = 91.1°$ (19–21). $LiCr(WO_4)_2$ is isostructural with $LiFe(WO_4)_2$ wolframite described in the space group $C2/c$ (C_{2h}^6) with $Z = 4$ and lattice parameters $a = 9.26$ Å, $b = 11.38$ Å, $c = 4.91$ Å, $\beta = 90.3°$ (20, 22). The coordination of tungsten ions in these compounds is octahedral. This arrangement consists of distorted octahedra connected by common edge forming chains along the c axis. The site symmetries of the M^+, Cr^{3+}, and W^{6+} atoms are C_2, C_2, and C_1, respectively.

In all compounds studied the chromium (III) ions are surrounded by six oxygen atoms. The structure of all crystals was checked by means of the X-ray diffraction (XRD) technique. In the temperature range 20–300 K they are stable and do not exhibit any structural phase transitions.

B. Phonon Properties

The infrared and Raman scattering spectra of the title compounds are shown in Figs. 1 and 2. Table 1 compares the energy regions for internal ν_1–ν_4 modes of the molybdate and tungstate anions as well as for optical external phonons. The following conclusions can be drawn from these results:

1. The internal vibrational modes of the scheelite-type crystals ($LiCr(MoO_4)_2$, $NaCr(MoO_4)_2$, $KCr(MoO_4)_2$, and $CsCr(MoO_4)_2$) consist of two groups corresponding to the stretching and bending vibrations of the molybdate anion. The number of IR and Raman lines in these multiplets fits well with those predicted by the theory based on factor group analysis (23, 24).

2. The internal vibrations of the wolframite-type compounds ($LiCr(WO_4)_2$ and $NaCr(WO_4)_2$) reflect structural

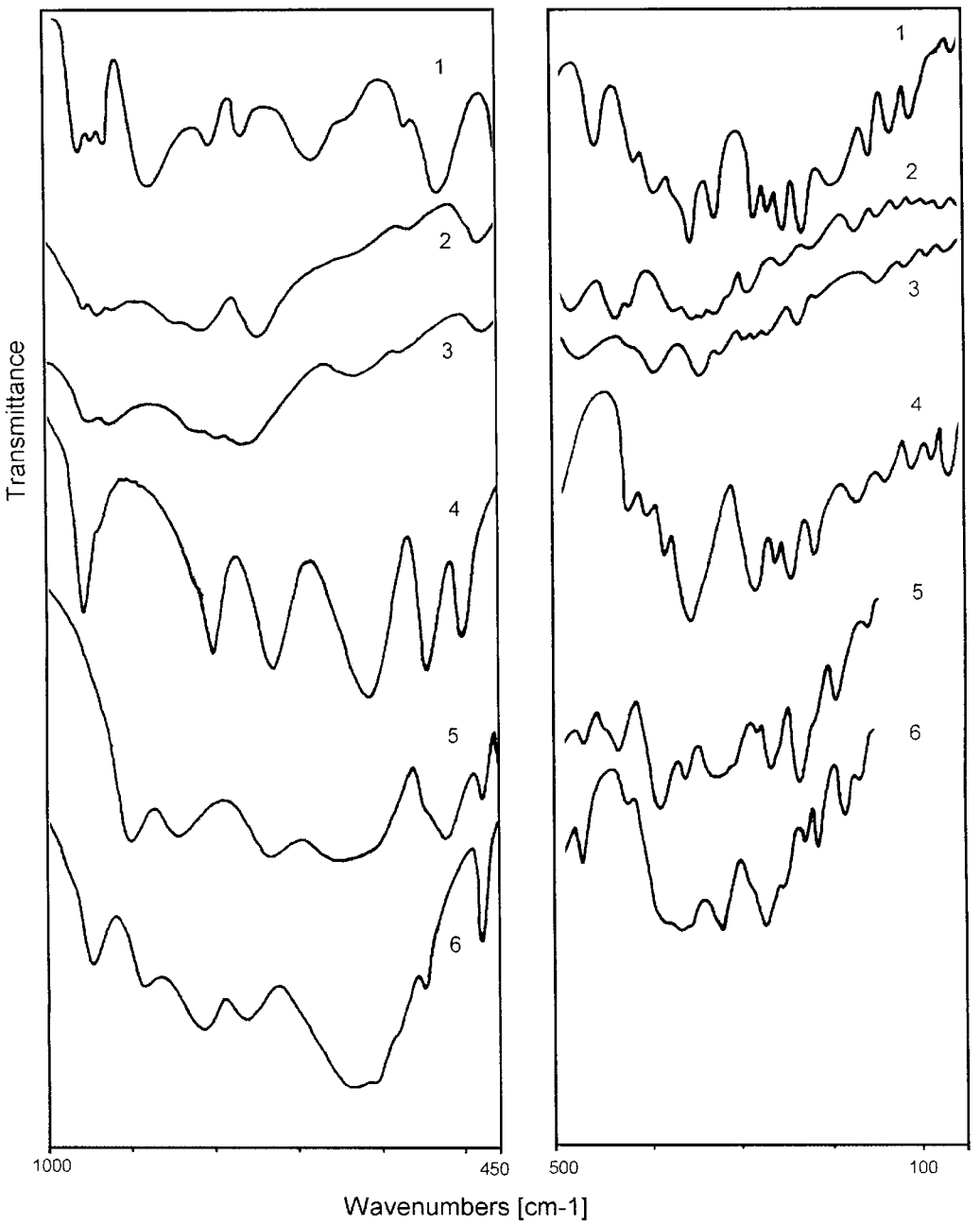

FIG. 1. IR spectra for $LiCr(MoO_4)_2$ (1), $NaCr(MoO_4)_2$ (2), $KCr(MoO_4)_2$ (3), $CsCr(MoO_4)_2$ (4), $LiCr(WO_4)_2$ (5), and $NaCr(WO_4)_2$ (6).

differences as compared to the scheelite-type crystals. This modification has a relatively high degree of condensation of oxygen atoms around the W^{VI} ions and dense packing of the coordination polyhedra in the unit cell. The resulting coordination number (CN) equals six because the tungstate ions are additionally connected to each other by means of intermolecular interactions of the $W/^{O}{}_{O}/W$ type. The characteristic vibrational bands corresponding to this structural fragment appear at the 500–700 cm^{-1} and 220–280 cm^{-1} regions and are assigned to stretching and bending modes of the $W/^{O}{}_{O}/W$ unit, respectively.

3. Optical external phonons are observed in the IR and RS spectra of the compounds studied at the wavenumbers below 250 cm^{-1}. The exchange of the M^+ (Li^+, Na^+, K^+, Cs^+) ions causes a frequency shift toward smaller wavenumbers. These changes allow us to propose the assignment of the respective translational phonons to the following vibrational regions: T′(Li^+) 190–210, T′(Na^+)

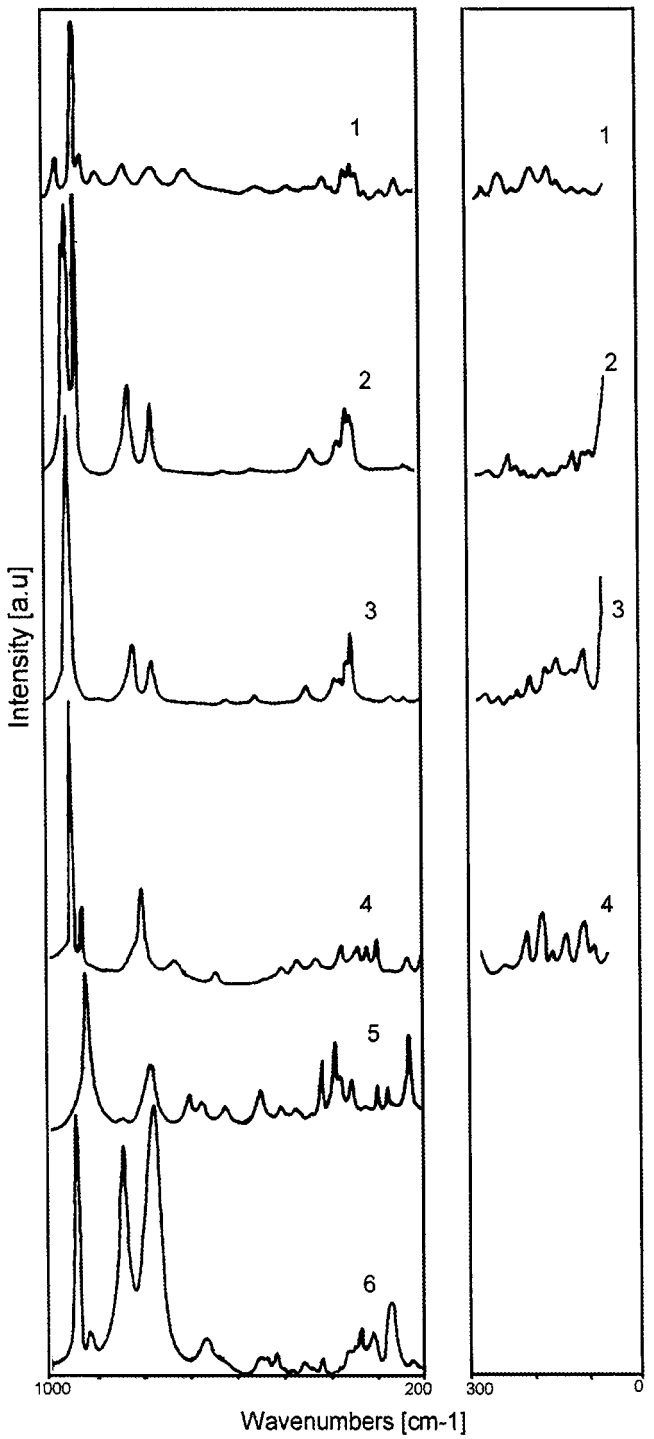

FIG. 2. Raman spectra for $LiCr(MoO_4)_2$ (1), $NaCr(MoO_4)_2$ (2), $KCr(MoO_4)_2$ (3), $CsCr(MoO_4)_2$ (4), $LiCr(WO_4)_2$ (5), and $NaCr(WO_4)_2$ (6).

170–190, $T'(K^+)$ 150–160, $T'(Cs^+)$ 160–180, and $T'(Cr^{3+})$ 110–170 cm^{-1}. The translational phonons $T'(MoO_4)$ and $T'(WO_4)$ are observed at 100–160 and 80–130 cm^{-1} and those of librational type at 200–240 and 190–250, respectively.

4. The numbers of the internal and external phonons being active in the vibrational spectra reflect the symmetry of the M^{I} (C_1, C_2), M^{III} (C_1, C_2 and C_i), and M^{VI} (C_1) ions in the respective unit cells (Table 1). The low symmetry of the Cr^{III} sites in the CrO_6 polyhedron has important consequences for the electron and ESR spectra of these materials.

C. Absorption and Emission Spectra

The absorption spectra of the concentrated $M^{I}Cr(MoO_4)_2$ scheelites were in general difficult to measure. It was only possible to cut the $KCr(MoO_4)_2$ crystal and measure the absorption spectra. For the rest of the crystals the information about electronic absorption transition could be obtained by means of diffuse reflectance (DR) technique.

The discussion of electronic absorption transition will be given following the data obtained from the diffuse reflectance spectra measured at room temperature. They are shown in Fig. 3. The characteristic energy features associated with the maxima of $^4A_2$–$^4T_1$ and $^4A_2$–$^4T_2$ transitions are listed in Table 2. The observed bands were not homogeneously broadened. We have found that the maxima of absorption bands of $^4A_2$–$^4T_1$ and $^4A_2$–$^4T_2$ transitions of molybdate scheelites $M^{I}Cr(MoO_4)_2$ were shifted toward shorter wavelengths with increasing ionic radius of the M^{I} ion. The Dq and B parameters were calculated from the electronic transitions using a standard procedure in which the fitting of the $^4T_1$, $^4T_2$, and ^2E_g energy levels was performed. The energy value of the $^4T_2$ level was reduced to the minimum of the parabola, i.e., to the point $E(^4T_2)$–$\frac{1}{2}$ Stokes shift. The values of the spectroscopic parameters are listed in Table 2. One can note that with increase in the ionic radius the magnitude of the B parameter increases. This parameter was also, respectively, larger for tungstate scheelites than for molybdate scheelites. Following the determined Dq and B parameters, we have listed in Table 2 the Dq/B ratio parameters which characterize the ligand field strength. As known, the ratio $Dq/B < 2.3$ characterizes the weak ligand field under which the $^4T_2$ state lies below the doublet ^2E state and only the broad band fluorescence $^4T_2$–$^4A_2$ is observed. In the case of the intermediate ligand field $Dq/B > 2.3$ both the fluorescence and phosphorescence of ^2E–$^4A_2$ may be observed. An inspection of Table 2 allows us to conclude that the Dq/B ratios are slightly below 2.3, and in principle for molybdate scheelites both emission transitions should be observed. One can note that for tungstates the respective ratios are significantly smaller (a weak ligand field limit), and only the fluorescence could be observed.

The emission spectra of scheelites were measured at room and low temperatures. They are of weak intensity because of the strong concentration quenching and ionic pair creation.

TABLE 1

Assignments	$LiCr(MoO_4)_2$	$NaCr(MoO_4)_2$	$KCr(MoO_4)_2$	$CsCr(MoO_4)_2$	$LiCr(WO_4)_2$	$NaCr(WO_4)_2$
ν_1 ($MO_{4\text{ or }6}$)	930–966	919–955	919–945	921–958	901–921	882–948
ν_2 ($MO_{4\text{ or }6}$)	812–885	756–845	769–825	795–810	782–844	810–844
ν ($M^{O}_{O}M$)	533–778	555–642	543–638	485–744	475–743	459–790
ν_3, ν_4 ($MO_{4\text{ or }6}$)	308–458	321–480	324–478	305–441	300–452	301–419
δ ($M^{O}_{O}M$)	220–280	238–304	235–284	218–274	232–285	223–270
L ($MO_{4\text{ or }6}$)	150–192	113–164	116–165	143–206	158–195	183–200
T′(M^{+})	266–332	219–242	235–260	92–143	311–452	223–351
T′(Cr^{3+})	178–192	158–242	165–237	192–252	223–285	200–270
T′(M^{6+})	53–130	50–140	69–148	50–143	158	131–147

The spectra are shown in Fig. 4. They are characterized by the broad bands assigned to the $^4T_2$–$^4A_2$ fluorescence transition. It was observed that with increased ionic radius of the M^I ion the energy of fluorescence increased, 10457 cm^{-1} for $LiCr(MoO_4)_2$ and 11105 cm^{-1} for $CsCr(MoO_4)_2$. This trend is not observed for $CsCr(MoO_4)_2$ where the lowest fluorescence energy was observed. It is due probably to the significantly larger Stokes shift (see Table 2). The results displayed in Figs. 3–5 clearly show that the Cr(III) ions in the compounds studied are distributed over at least two cationic sites. Therefore in Table 2, two values for the $^4T_2$, $^4T_1(^4F)$, and ^2E levels, as well as for the B, Dq, and Dq/B parameters, are listed. We have measured the fluorescence decay curves. The observed profiles were nonexponential due to the strong concentration quenching and contribution of different Cr(III) sites to the total fluorescence. We have estimated the decay times from the longer decay time components. They are listed in Table 2. One can note that the longest lifetime was measured for $KCr(MoO_4)_2$ to be 100 μs. The shortest lifetimes were observed for tungstate scheelites, about 10 μs, for which the Cr–Cr distances are respectively smaller. The lifetimes measured were associated with the fluorescence transition $^4T_2$–$^4A_2$. The nonexponentiality can

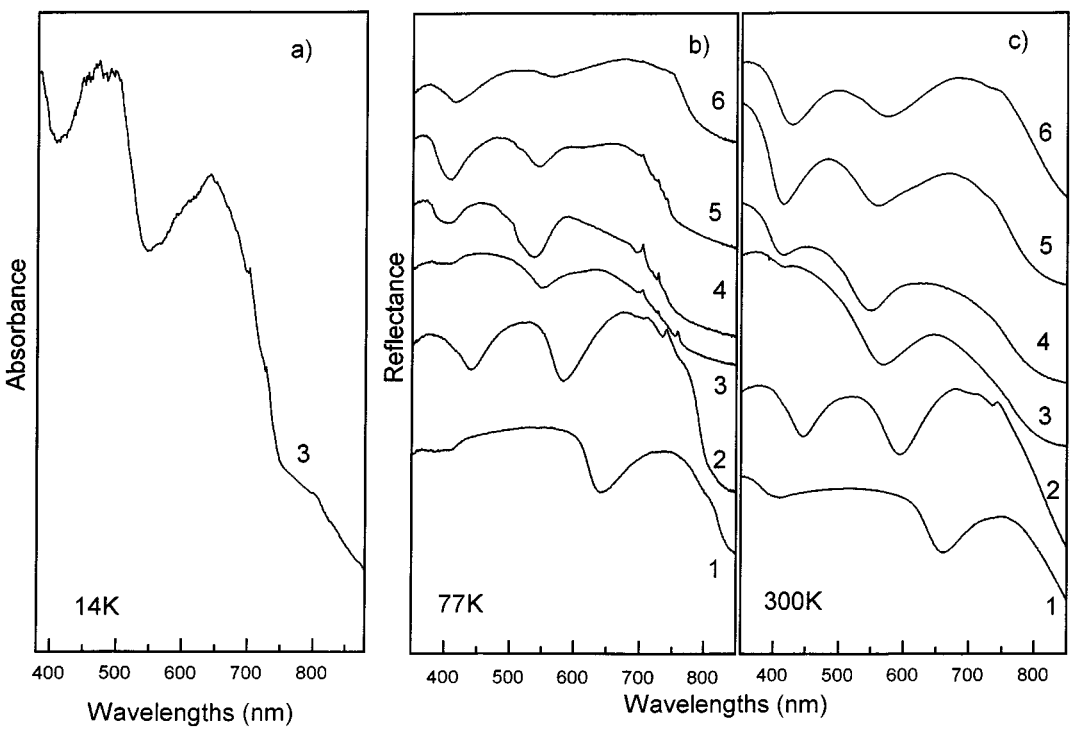

FIG. 3. Diffuse reflectance spectra for $LiCr(MoO_4)_2$ (1), $NaCr(MoO_4)_2$ (2), $KCr(MoO_4)_2$ (3), $CsCr(MoO_4)_2$ (4), $LiCr(WO_4)_2$ (5), and $NaCr(WO_4)_2$ (6).

TABLE 2

	$LiCr(MoO_4)_2$	$NaCr(MoO_4)_2$	$KCr(MoO_4)_2$[a]	$CsCr(MoO_4)_2$	$LiCr(WO_4)_2$	$NaCr(WO_4)_2$
Ionic radius of M^I ion [nm]	0.068	0.097	0.133	0.167	0.068	0.097
$^4T_1(^4P)$ (cm^{-1})	28090	30300	27550	26810	29415	26525
	20500	20813	22026	21900		20200
$^4T_1(^4F)$ (cm^{-1})					20000	19900
	19350	20000	20408	20400		19100
$^4T_2$ (cm^{-1})	14620	14920	15870	15460	14710	13390
$^2T_1$ (cm^{-1})		13755	13812	13755		
		14224	14204	14224		
^2E (cm^{-1})			13200			
	13078	13365	13552	13550	13477	13477
	1470	1492	1590	1570		1460
D_q (cm^{-1})					1360	1400
	1333	1379	1430	1415		1299
	632	650	629	654		650
B (cm^{-1})					686	601
	577	587	605	617		552
	2.11	2.11	2.27	2.16		1.99
Dq/B					1.98	2.33
	2.54	2.54	2.62	2.54		2.64
E_M[b] (cm^{-1})	2873	3017	3195	4011	3100	2810
ΔE[b] (cm^{-1})	−1620	−1232	−850	−1405	−1426	−1891
$\tau(^4T_2)$ (μs)	18	22	100	60	10	7

[a]Measured at 14 K.
[b]Calculated for the weak ligand field sites.

be attributed to the concentration quenching (a simultaneous contribution of donor–donor (migration) and donor–acceptor interactions) and the contribution of different Cr(III) sites. The measured lifetimes can not be interpreted as a superposition of two exponentials. We have only distinguished the longest components for comparative purposes in the table.

The weak phosphorescence ^2E–$^4A_2$ transitions were observed only for $CsCr(MoO_4)_2$ and $KCr(MoO_4)_2$ scheelites at 14 K (Fig. 5). The phosphorescence energies coincide very well with some sharp features in the absorption spectra. For the other molybdates the phosphorescence could not be observed due to the strong nonradiative relaxation. In the case of tungstates the phosphorescence can not be observed because of a weak ligand field character.

D. ESR Studies

Figure 6 shows the room temperature ESR spectra of the compounds studied and their temperature dependencies down to 4 K. The g and ΔH_{pp} parameters obtained from these measurements are given in Table 3.

The spectra show the lines arising from the well-known Cr^{III} center, having a giromagnetic factor $g \cong 1.97$. For all samples the half-width of the signal reveals the temperature evolution. For the lithium, sodium, and potassium molybdates, as well as for the sodium tungstate, the ΔH_{pp} factor slightly decreases in the temperature range from 300 to 100 K. As the temperature is decreased from 100 K the signal width significantly increases taking at the lowest point 4.2 K values several times greater (Table 3). For the caesium molybdate the accelerated increase of this factor is observed in the whole temperature range from 300 to 4.2 K. On the other hand, the signal of the lithium tungstate reveals the complex contour which can be divided into two components, one of which has nearly unchanged signal width, and the other has increasing band width (Fig. 6).

The broadening of the ESR signal below 100 K in the described manner suggests that magnetic ordering appears in the compounds studied. The presence of magnetic phase transition follows also from magnetic susceptibility measurements.

E. Magnetic Properties

The magnetic properties of all molybdates and lithium tungstate are very similar. The temperature and magnetic field variations of the magnetic susceptibility, as well as

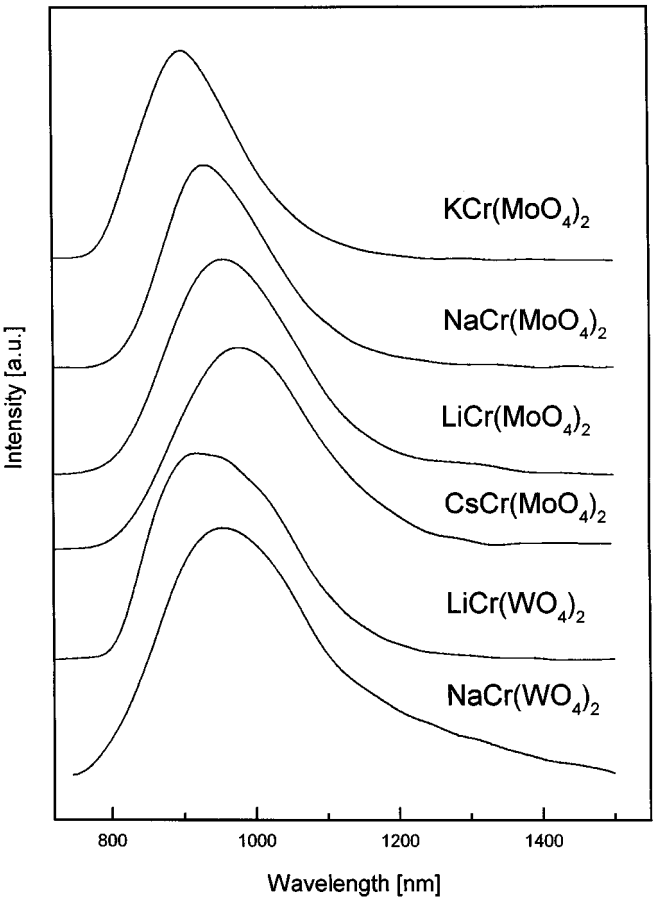

FIG. 4. The 15 K emission spectra of scheelite-like crystals.

$\chi_m^{-1}(T)$ dependencies for these compounds are shown in Figs. 7–12.

The $\chi(T)$ plots in all cases exhibit characteristic maxima at temperatures close to 20 K for lithium, sodium, potassium molybdates, and lithium tungstate. For the caesium molybdate and sodium tungstate the antiferromagnetic ordering appears below 7.01 and 80.1 K, respectively. For all compounds, except sodium tungstate, it could be assumed

TABLE 3

	g factor			ΔH_{pp}			
Compound	100–300 K	50 K	4.2 K	100–300 K	50 K	4.2 K	T_N
$LiCr(MoO_4)_2$	1.9518	1.9543		28.72	35.28	296	20.07
$NaCr(MoO_4)_2$	1.9430	1.9430	1.9345	49.5	56.9	74.1	20.02
$KCr(MoO_4)_2$	2.0796	1.9626	1.9372	105.0	128.3	246.3	18.01
$CsCr(MoO_4)_2$	2.0822	1.9237	1.9267	101.0	163.7	195.0	7.01
$LiCr(WO_4)_2$	1.9590	1.9077		54.2	51.6		20.07
	1.9984	1.9077	1.8179	123.7	241.8	272.0	
$NaCr(WO_4)_2$	1.9536	1.9541		30.8	42.5		80.10

TABLE 4

Compound	Neel point T_N (K)	Temperature range where Curie–Weiss law is obeyed (K)	$\chi_0 \times 10^4$	C	Θ_p (K)	μ_{eff} (μ_B)
$LiCr(MoO_4)_2$	20.07	30–300	5.6	1.797	− 64.1	3.79
$NaCr(MoO_4)_2$	20.02	50–300	10.3	1.532	− 34.9	3.50
$KCr(MoO_4)_2$	18.01	30–300	9.1	1.476	− 33.6	3.44
$CsCr(MoO_4)_2$	7.01	30–300	8.5	1.583	− 1.2	3.56
$LiCr(WO_4)_2$	20.07	30–300	0.9	1.625	− 27.1	3.61
$NaCr(WO_4)_2$	80.10					

that above T_N the susceptibility follows the Curie–Weiss law in a temperature range up to 220 K for the molybdates and 300 K for the lithium tungstate. For the molybdates above 220 K $\chi_m^{-1}(T)$ dependence deviates from a straight line behavior. This deviation disappears when the fitting procedure in the form $\chi_m^{-1}(T) = \chi_0 + C/T - \Theta$ is used. Here,

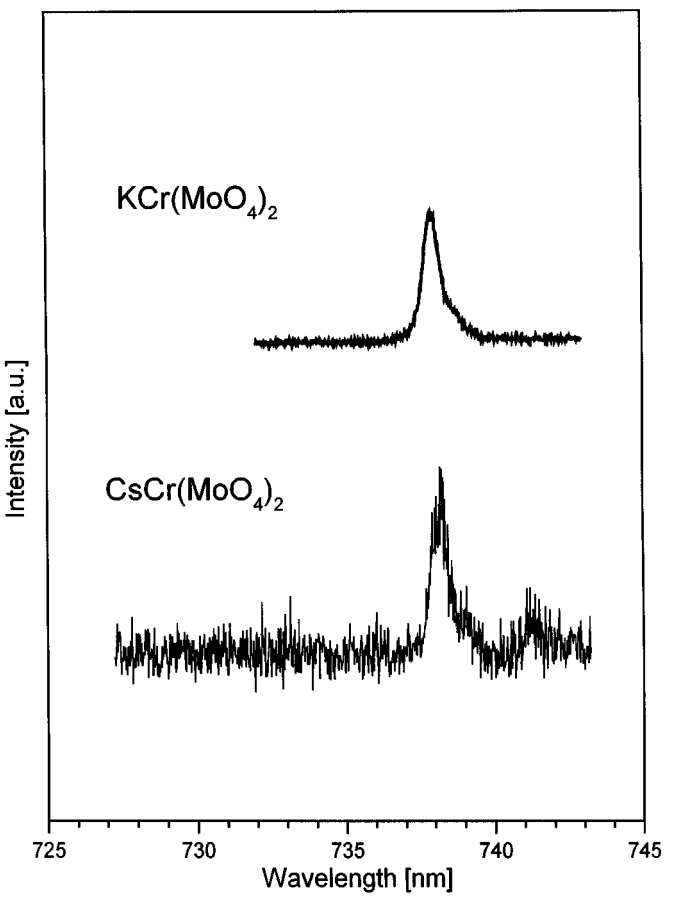

FIG. 5. The R_1 lines observed in the emission spectrum at 15 K. A highly sensitive photomultiplier was used. The half-width of the line is 7 cm^{-1}.

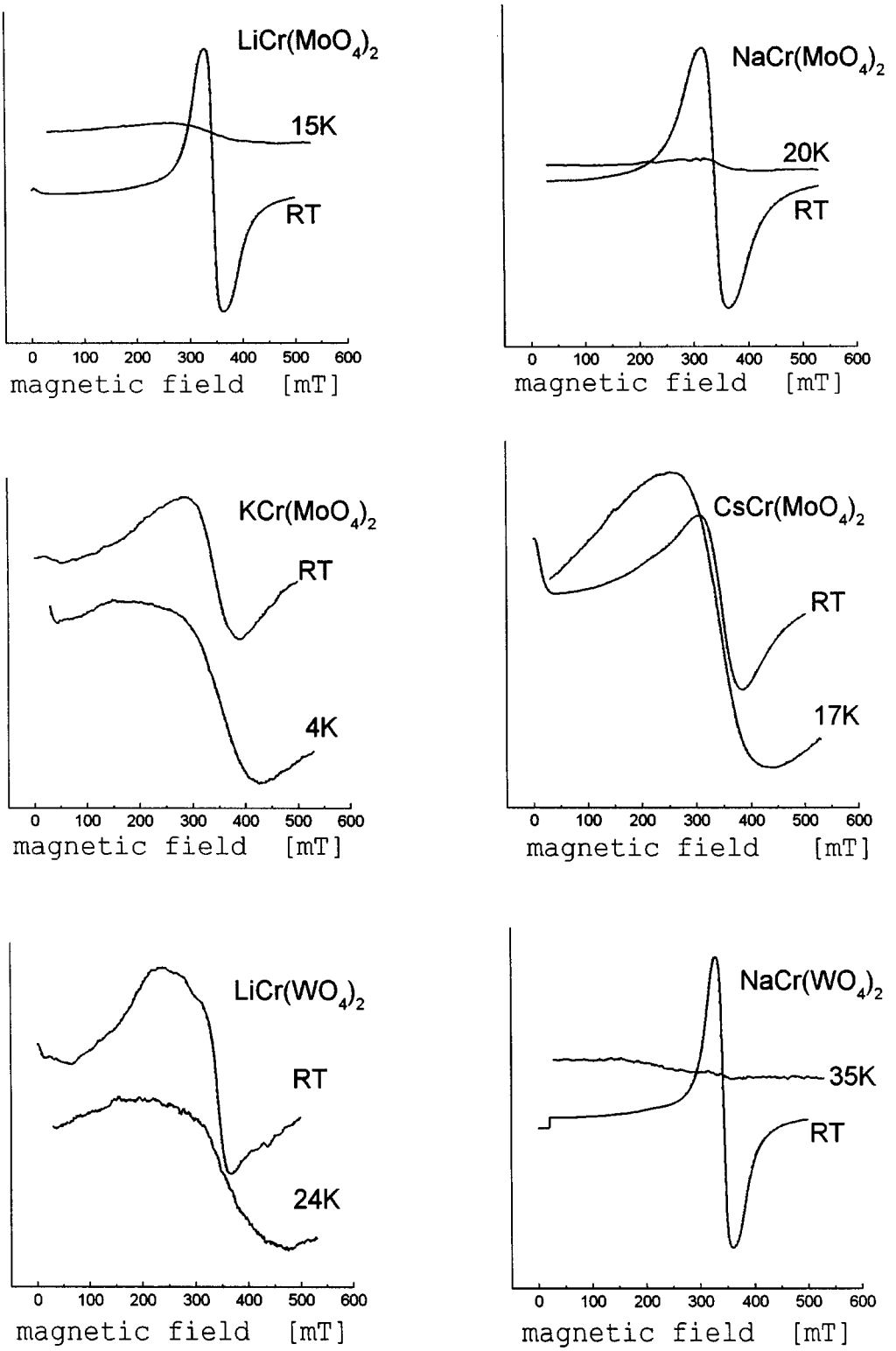

FIG. 6. The ESR spectra for $LiCr(MoO_4)_2$ (1), $NaCr(MoO_4)_2$ (2), $KCr(MoO_4)_2$ (3), $CsCr(MoO_4)_2$ (4), $LiCr(WO_4)_2$ (5), and $NaCr(WO_4)_2$ (6).

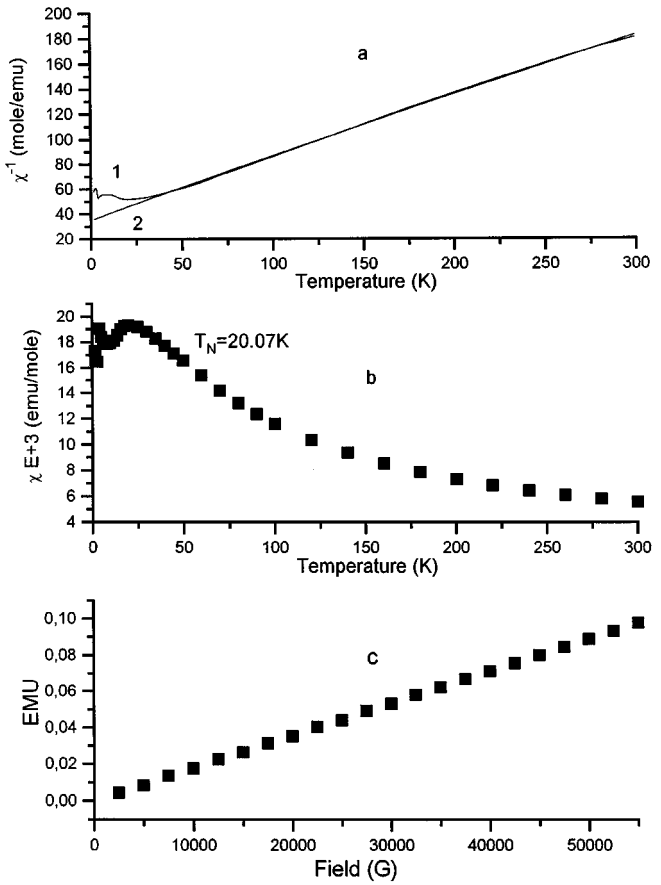

FIG. 7. The temperature dependence of χ^{-1} (a) (1, experimental data; 2, line obtained from the fitting procedure) and χ (b), and the field dependence of χ (c) for $LiCr(MoO_4)_2$.

χ_0 denotes the material dependent parameter, which accounts for possible conduction-electron paramagnetic and core-electron diamagnetic contributions as well as for the temperature-independent van Vleck contribution to the total measured magnetic susceptibility. The least square fits of the experimental $\chi(T)$ variations for these compounds are shown in Figs. 7a–11a.

The magnetic properties of the sodium tungstate is significantly higher (80.1 K), and the $\chi(T)$ and $\chi^{-1}(T)$ curves could not be fitted to the straight line expression.

The effective magnetic moments evaluated for the compounds studied in the fitting procedure equal 3.6–3.9 MB per Cr atom and the paramagnetic Curie temperatures vary in the range 11.1–69.3 K. The values μ_{eff} are very close to those expected for a free Cr^{III} ion.

The magnetic field dependencies of the magnetic susceptibility are linear for all compounds studied. This means that the exchange interactions between the spins play an important role in these materials.

The magnetic parameters obtained for the materials studied are collected in Table 4.

SUMMARY AND OUTLOOK

This work initiates studies of chromium(III)-doped double molybdates and tungstates of the $M^{I}M^{III}_{1-x}Cr_x(M^{VI}O_4)_2$ family. The aim of these studies is to assess their suitability as tunable laser gain media. In all six compounds studied, efficient pumping in the $^4A_2 \rightarrow {}^4T_1$ band is possible with the major resonance lines of the Kr^+ laser. The $^4A_2 \rightarrow {}^4T_2$, $^4T_1$ bands cover nearby all of the visible region and, as has been proved for other Cr^{3+}-based laser systems, are good for flash-lamp pumping. The luminescence output at 77 K for the compounds studied is similar to that of Cr^{3+} in beryllium spinel $BeAl_2O_4$, exhibiting emission from both ^2E and $^4T_2$ states. Therefore, the long-lived ^2E state can act as an efficient storage level for laser action from the $^4T_2$ level.

These compounds also offer other interesting possibilities. The magnetic and ESR studies reveal antiferromagnetic ordering and strong exchange interactions in these materials.

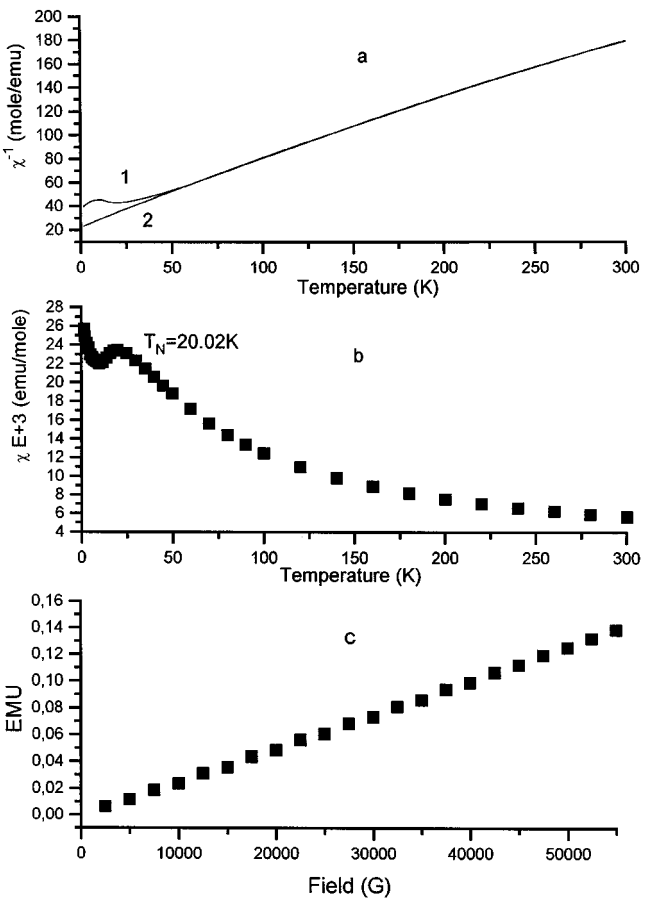

FIG. 8. The temperature dependence of χ^{-1} (a) (1, experimental data; 2, line obtained from the fitting procedure) and χ (b), and the field dependence of χ (c) for $NaCr(MoO_4)_2$.

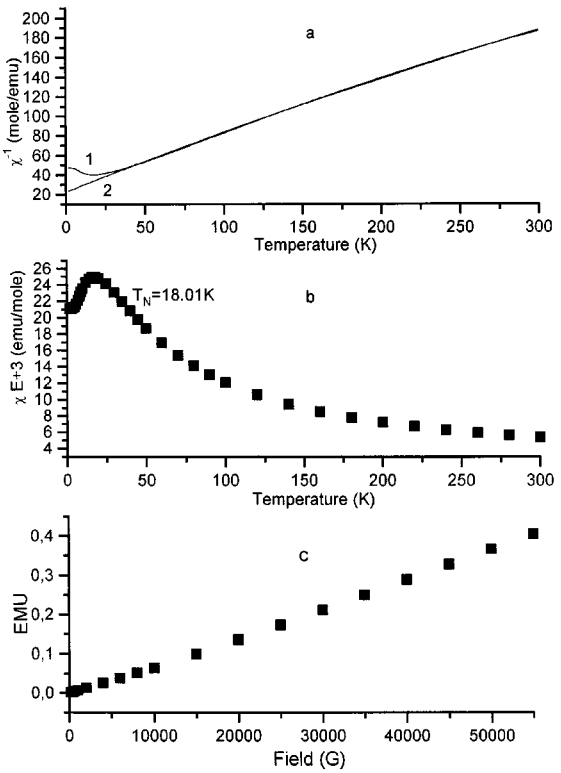

FIG. 9. The temperature dependence of χ^{-1} (a) (1, experimental data; 2, line obtained from the fitting procedure) and χ (b), and the field dependence of χ (c) for $KCr(MoO_4)_2$.

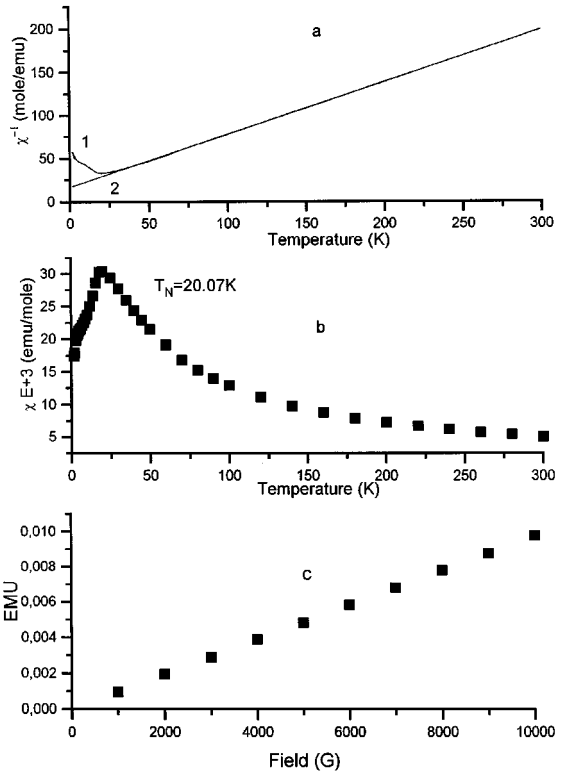

FIG. 11. The temperature dependence of χ^{-1} (a) (1, experimental data; 2, line obtained from the fitting procedure) and χ (b), and the field dependence of χ (c) for $LiCr(WO_4)_2$.

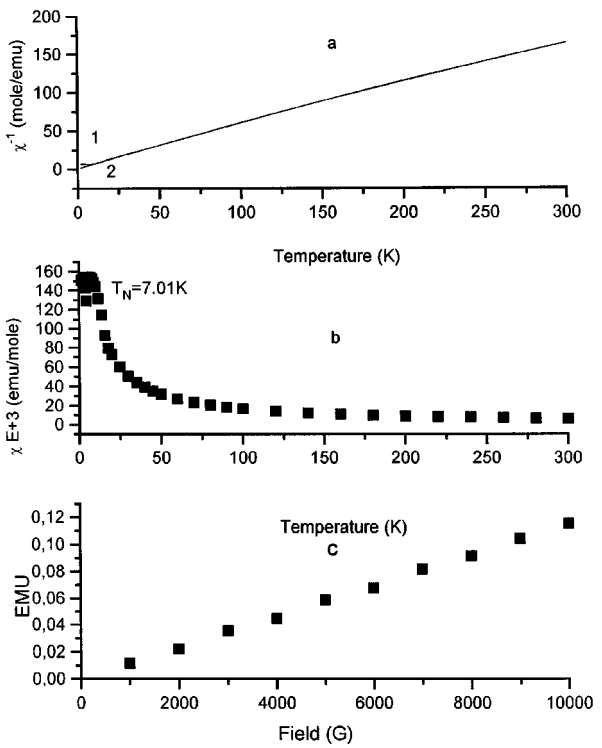

FIG. 10. The temperature dependence of χ^{-1} (a) (1, experimental data; 2, line obtained from the fitting procedure) and χ (b), and the field dependence of χ (c) for $CsCr(MoO_4)_2$.

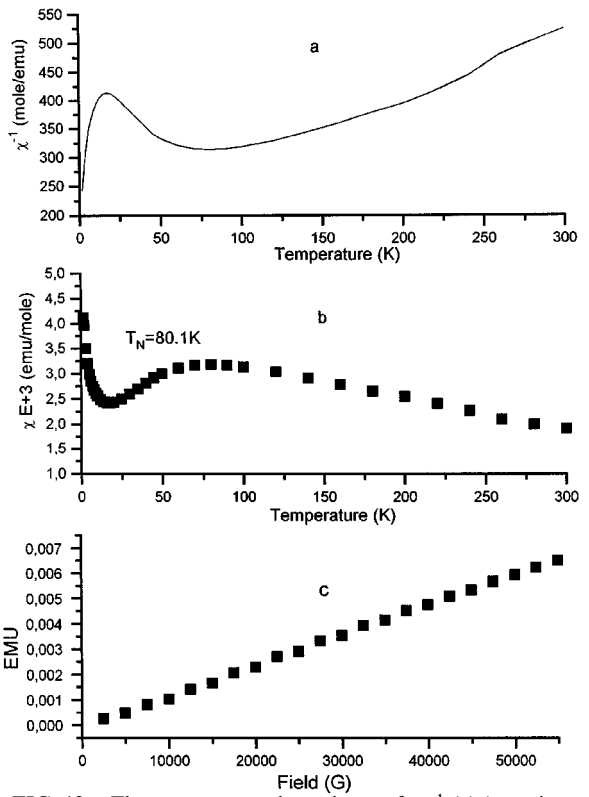

FIG. 12. The temperature dependence of χ^{-1} (a) (experimental data) and χ (b), and the field dependence of χ (c) for $NaCr(WO_4)_2$.

ACKNOWLEDGMENT

This work was supported by the Polish State Committee for Scientific Research under grant 3T09A 057 13.

REFERENCES

1. V. Petricevic, S. K. Gayen, and R. R. Alfano, *Appl. Phys. Lett*. **53,** 2590 (1988).
2. H. R. Verdun, L. M. Thomas, D. M. Andrauskas, and T. Mc Collum, *Appl. Phys. Lett*. **53,** 2593 (1988).
3. N. I. Borodin, V. A. Zhitnyuk, A. G. Okhrimchuk, and A. V. Shestakov, *Izv. Akad*, *Nauk SSSR Ser. Fiz*. **54,** 1500 (1990).
4. W. Jia, H. Eilers, W. M. Dennis, W. M. Yen, and A. V. Shestakov, "Proceedings, Advanced Solid State Lasers" (L. L. Chase and A. A. Pinto, Eds.), Vol. 13, pp. 31–33. Optical Society of America, Washington, DC, 1992.
5. H. Eilers, W. M. Dennis, W. M. Yen, S. Kück, K. Peterman, G. Huber, and W. Jia, *IEEE J. Quantum Electron*. **29,** 2508 (1993).
6. A. A. Kaminskii, "Laser Crystals," Springer Series in Optical Studies. Springer-Verlag, Berlin, 1981.
7. G. Blasse, *Struct. Bond*. **42,** 1 (1980).
8. W. I. F. David and A. M. Glazer, *Phase Transition* **1,** 155 (1979); W. I. F. David, *Mater. Res. Bull*. **18,** 749 (1983).
9. A.W. Sleigh, H. Y. Chen, A. Ferretti, and D. E. Cox, *Mater. Res. Bull*. **14,** 1571 (1979).
10. S. Tsunekawa and H. Takei, *J. Phys. Soc. Jpn*. **40,** 1523 (1976); S. Tsunekawa and H. Takei, *J. Cryst. Growth* **38,** 55 (1977).
11. J. Sapriel, *Phys. Rev. B* **12,** 5128 (1975).
12. A. Jayaraman, B. Battloy, and L. G. van Uitert, *Phys. Rev. B* **28,** 4474 (1983); A. Jayaraman, B. Battloy, and L. G. van Uitert, *Phys. Rev. B* **31,** 5423 (1983).
13. J. Hanuza, A. Benzar, A. Haznar, M. Maczka, A. Pietraszko, and J. H. van der Maas, *Vibrational Spectrosc*. **12,** 25 (1996).
14. P. V. Klevtsov and R. F. Klevtsova, *Zh. Struk. Khim*. **18,** 419 (1977).
15. L. P. Soloveeva and R. F. Borisov, *Kristallogr*. **15,** 577 (1970).
16. P. V. Klevtsov, L. P. Kozeeva, and R. F. Klevtsova, *Zh. Neorg. Khim*. **20,** 2999 (1975).
17. P. V. Trunov and V. A. Efremov, *Zh. Neorg. Khim*. **16,** 2026 (1971).
18. R. F. Klevtsova and P. V. Klevtsov, *Kristallogr*. **15,** 953 (1970).
19. I. G. Avaeva, V. B. Kravtsenko, and T. N. Kobyzeva, *Neorg. Mater*. **8,** 586 (1972).
20. R. Salmon, A. Casalot, G. Le Flem, and P. Hagenmuller, *Mater. Res. Bull*. **5,** 341 (1970).
21. P. V. Klevtsov and R. F. Klevtsova, *J. Solid State Chem*. **2,** 278 (1970).
22. P. V. Klevtsov and R. F. Klevtsova, *Kristallogr*. **15,** 294 (1970).
23. J. Hanuza and M. Mączka, *Vibrational Spectrosc*. **7,** 85 (1994).
24. J. Hanuza, M. Mączka, and J. H. van der Maas, *J. Solid State Chem*. **117,** 177 (1995).